Quantum signatures of transitions from stable fixed points to limit cycles in optomechanical systems

Qing Xia Meng [1,2] Zhi Jiao Deng [1,2,*] Zhigang Zhu [3,4] and Liang Huang [4]

[1] *Department of Physics, College of Liberal Arts and Sciences, National University of Defense Technology, Changsha 410073, China*

[2] *Interdisciplinary Center for Quantum Information, National University of Defense Technology, Changsha 410073, China*

[3] *Department of Physics, Lanzhou University of Technology, Lanzhou, Gansu 730050, China*

[4] *School of Physical Science and Technology and Key Laboratory for Magnetism and Magnetic Materials of MOE, Lanzhou University, Lanzhou, Gansu 730000, China*

(Received 22 July 2019; accepted 15 January 2020; published 25 February 2020)

Optomechanical systems, due to its inherent nonlinear optomechanical coupling, owns rich nonlinear dynamics of different types of motion. The interesting question is that whether there exist some common quantum features to infer the nonlinear dynamical transitions from one type to another. In this paper, we study the quantum signatures of transitions from stable fixed points to limit cycles in an optomechanical phonon laser system. Our calculations show that the entanglement of stable fixed points in the long run does not change with time; however, it oscillates periodically with time at the mechanical vibration frequency for the limit cycles. Most strikingly, the entanglement quite close to the boundary line remains constant, and it is very robust against thermal phonon noise, as strong indications of this particular classical transitions.

DOI: 10.1103/PhysRevA.101.023838

I. INTRODUCTION

Optomechanics, which deals with the nonlinear dynamics of coupled radiation fields and mechanical vibrations, has attracted huge recent attention [1]. Ground-state cooling is expected in many applications [2], therefore it is very important to make clear the quantum states and quantum properties of systems at low temperature. Due to the intrinsic nonlinear nature, the optomechanical system owns rich nonlinear dynamics such as bistability, limit cycle, and chaos [3]. When the temperature goes down, the influence of quantum fluctuations becomes prominent and various quantum properties would also appear. An interesting question is that when the classical nonlinear dynamics changes from one type to another, are there any signatures of these transitions in the corresponding quantum system?

There are already several related works [4–8] in this regard. Reference [4] shows that the time evolution of quantum entanglement is periodic for limit cycles, while it exhibits beat-like behavior with two distinct frequencies for quasiperiodic motion. And the most surprising feature is that the entanglement vanishes abruptly at the boundary of these two motions, as a strong quantum fingerprints of this particular transition. In a system of two coupled optomechanical cavities, the entanglement of two mechanical modes reveals a second-order phase transition type of change at the critical point from their in-phase to antiphase synchronization [5]. Reference [6] proposes new measures for quantum synchronization, and points out that their data are not sufficient to clarify the functional relationship between quantum synchronization and quantum discord. Another group also investigates the measure for quantum synchronization, and they find out that quantum discord behaves similarly to the measure of quantum synchronization based on their concrete optomechanical model [7]. The entanglement in the bistable regime has also been analyzed, which will jump discontinuously along the hysteresis loop [8]. Most of the previous works discuss only one set of parameters passing through the transition point. It is natural to ask whether the changing quantum properties show common features no matter where to cross the boundary of two different types of nonlinear motions.

In this article, we investigate the quantum signatures of transitions from stable fixed points to limit cycles. Our discussions is based on a two-dimensional phase diagram of an optomechanical phonon laser model [9]. The phonon laser, also referred to as a mechanical self-sustained oscillation [1], is essentially a limit cycle from the perspective of nonlinear dynamics. It has been studied thoroughly [10–18] and realized in recent experiments [9,19,20] in the context of optomechanics. The phonon laser in Ref. [9] is generated by the parametric down conversion process [21]. The system will reach a stable fixed point in the long run when the driving power is not very strong but undergoes a limit cycle motion once above a certain driving threshold. Our aim is to look for the common changing features of quantum entanglement around the boundaries of these two nonlinear motions. To do that, we choose several different paths to cross the boundaries. Our calculations show that the entanglement for the stable fixed points does not change with time, while it oscillates at the mechanical frequency for the limit cycles. The most striking phenomenon is that the entanglement of those points very close to their boundary line is a constant, and it is very robust to the mechanical thermal noise, as obvious quantum signatures of this nonlinear dynamical transitions from one to another. Our paper is organized as follows, in Sec. II, we introduce the physical model and derive its equations of motion. In Sec. III, we first present the classical equations of

*dengzhijiao926@hotmail.com

motion and give a two-dimensional phase diagram regarding the strength and detuning of the driving laser, and then discuss the classical nonlinear dynamics along three different paths in the phase diagram. In Sec. IV, we show the general procedures to calculate the quantum entanglement and study how it will change along the three above-mentioned paths. In Sec. V, we summarize our results.

II. PHYSICAL SYSTEM

The optomechanical system in the experiment of Ref. [9] consists of two coupled cavity modes, one of which is coupled to a mechanical mode by the radiation pressure force, and the other is driven by an input laser. The Hamiltonian of the whole system is

$$\hat{H} = \hbar\omega_a(\hat{a}_1^\dagger\hat{a}_1 + \hat{a}_2^\dagger\hat{a}_2) + \hbar J(\hat{a}_1^\dagger\hat{a}_2 + \hat{a}_1\hat{a}_2^\dagger) - \hbar g\hat{a}_2^\dagger\hat{a}_2\hat{q} + \frac{\hbar\omega_m}{2}(\hat{p}^2 + \hat{q}^2) + i\hbar\Lambda(\hat{a}_1^\dagger e^{-i\omega_L t} - \hat{a}_1 e^{i\omega_L t}), \quad (1)$$

where the two localized cavity modes have the same frequency ω_a, and their tunneling rate is denoted by J. The mechanical mode with frequency ω_m is coupled to cavity mode 2 by a constant coupling strength g. The operators $\hat{q} = \frac{1}{\sqrt{2}}(\hat{b}^\dagger + \hat{b})$, $\hat{p} = \frac{1}{\sqrt{2}i}(\hat{b} - \hat{b}^\dagger)$ represent the dimensionless position and momentum of the mechanical mode, respectively. The last term describes the driving of cavity mode 1 by a laser with frequency ω_L and amplitude Λ.

A proper analysis of the system must include photon losses in the cavity and the Brownian noise acting on the mechanical vibration. This can be accomplished by considering the following set of nonlinear Langevin equations [written in the interaction picture with respect to $\hbar\omega_L(\hat{a}_1^\dagger\hat{a}_1 + \hat{a}_2^\dagger\hat{a}_2)$] [22]:

$$\begin{aligned}
\dot{\hat{a}}_1 &= \Big(i\Delta - \frac{\kappa}{2}\Big)\hat{a}_1 - iJ\hat{a}_2 + \Lambda + \sqrt{\kappa}\hat{a}_{\mathrm{in},1},\\
\dot{\hat{a}}_2 &= \Big(i\Delta - \frac{\kappa}{2}\Big)\hat{a}_2 - iJ\hat{a}_1 + ig\hat{a}_2\hat{q} + \sqrt{\kappa}\hat{a}_{\mathrm{in},2},\\
\dot{\hat{q}} &= \omega_m\hat{p},\\
\dot{\hat{p}} &= g\hat{a}_2^\dagger\hat{a}_2 - \omega_m\hat{q} - \gamma_m\hat{p} + \hat{\xi}.
\end{aligned} \quad (2)$$

Here $\Delta = \omega_L - \omega_a$ denotes the laser detuning from the cavity resonance, γ_m is the mechanical damping rate, and κ is the optical intensity decay rate. The operators $\hat{a}_{\mathrm{in},1}$, $\hat{a}_{\mathrm{in},2}$ are the vacuum radiation input noise. Their mean values satisfy $\langle\hat{a}_{\mathrm{in},j}(t)\rangle = 0$, and their only nonzero correlation functions fulfill $\langle\hat{a}_{\mathrm{in},j}(t)\hat{a}_{\mathrm{in},j'}^\dagger(t')\rangle = \delta_{jj'}\delta(t-t')$ with $j = 1, 2$. The Hermitian Brownian noise operator $\hat{\xi}$ with zero mean value satisfies a delta-correlated function $\frac{1}{2}\langle\hat{\xi}(t)\hat{\xi}(t') + \hat{\xi}(t')\hat{\xi}(t)\rangle = \gamma_m(2\overline{n}+1)\delta(t-t')$ in the limit of high mechanical quality factor [4,7,23], i.e., $Q = \omega_m/\gamma_m \gg 1$, where $\overline{n} = [\exp(\frac{\hbar\omega_m}{k_B T}) - 1]^{-1}$ is the mean thermal phonon number at temperature T, and k_B is Boltzmann's constant.

The mechanism to generate the phonon laser can be understood more clearly if we transform to the basis with supermodes defined as $\hat{c}_1 = \frac{1}{\sqrt{2}}(\hat{a}_1 + \hat{a}_2)$, $\hat{c}_2 = \frac{1}{\sqrt{2}}(\hat{a}_1 - \hat{a}_2)$. The Langevin equations are now in the following forms:

$$\begin{aligned}
\dot{\hat{c}}_1 &= \Big(i(\Delta - J) - \frac{\kappa}{2}\Big)\hat{c}_1 + \frac{ig}{2}(\hat{c}_1 - \hat{c}_2)\hat{q} + \frac{\Lambda}{\sqrt{2}} + \sqrt{\kappa}\hat{c}_{\mathrm{in},1},\\
\dot{\hat{c}}_2 &= \Big(i(\Delta + J) - \frac{\kappa}{2}\Big)\hat{c}_2 - \frac{ig}{2}(\hat{c}_1 - \hat{c}_2)\hat{q} + \frac{\Lambda}{\sqrt{2}} + \sqrt{\kappa}\hat{c}_{\mathrm{in},2},\\
\dot{\hat{q}} &= \omega_m\hat{p},\\
\dot{\hat{p}} &= \frac{g}{2}(\hat{c}_1^\dagger\hat{c}_1 + \hat{c}_2^\dagger\hat{c}_2 - \hat{c}_1^\dagger\hat{c}_2 - \hat{c}_2^\dagger\hat{c}_1) - \omega_m\hat{q} - \gamma_m\hat{p} + \hat{\xi},
\end{aligned} \quad (3)$$

where $\hat{c}_{\mathrm{in},1} = \frac{1}{\sqrt{2}}(\hat{a}_{\mathrm{in},1} + \hat{a}_{\mathrm{in},2})$ and $\hat{c}_{\mathrm{in},2} = \frac{1}{\sqrt{2}}(\hat{a}_{\mathrm{in},1} - \hat{a}_{\mathrm{in},2})$, obeying similar correlation functions as for $\hat{a}_{\mathrm{in},1}$ and $\hat{a}_{\mathrm{in},2}$. The eigenfrequencies for the c_1 and c_2 modes in the interaction picture are $-(\Delta - J)$, $-(\Delta + J)$ respectively. If their frequency difference $2J$ is near resonant with the mechanical frequency ω_m, i.e., $2J \simeq \omega_m$, then an efficient driving of the c_1 mode with $\Delta \simeq J$ could lead to a parametric down conversion process via the interaction term $\hat{c}_1^\dagger\hat{c}_2\hat{b} + \hat{c}_2^\dagger\hat{c}_1\hat{b}^\dagger$, which means that, when one photon in the c_1 mode disappears, a photon in the c_2 mode and a phonon are born. When the driving is above the threshold power, coherent oscillation (i.e., mechanical lasing) would occur in the mechanical mode. Moreover, this two-mode squeezing interaction term will inevitably result in the quantum entanglement between the optical c_2 mode and the mechanical mode, as discussed in many previous works [24–31].

III. NONLINEAR DYNAMICS

Equation (3) in the regime of weak coupling $g \ll \kappa$ and moderate driving Λ can be solved by the mean-field approximation [1], in which quantum operators are separated into $\hat{O} = \langle\hat{O}\rangle + \delta\hat{O}$, where $\langle\hat{O}\rangle \equiv O$ is the mean field describing the classical behavior of the system, and $\delta\hat{O}$ is the quantum fluctuation with zero mean value around the classical orbit. In this section, we focus on the classical dynamics of the system. The equations of motion for the classical mean fields form a set of nonlinear differential equations given by

$$\begin{aligned}
\dot{c}_1 &= \Big[i(\Delta - J) - \frac{\kappa}{2}\Big]c_1 + \frac{ig}{2}(c_1 - c_2)q + \frac{\Lambda}{\sqrt{2}},\\
\dot{c}_2 &= \Big[i(\Delta + J) - \frac{\kappa}{2}\Big]c_2 - \frac{ig}{2}(c_1 - c_2)q + \frac{\Lambda}{\sqrt{2}},\\
\dot{q} &= \omega_m p,\\
\dot{p} &= -\omega_m q - \gamma_m p + \tfrac{1}{2}g(c_1^* c_1 + c_2^* c_2 - c_1^* c_2 - c_2^* c_1),
\end{aligned} \quad (4)$$

which is obtained by averaging both sides of Eq. (3) and approximates $\langle\hat{F}\hat{G}\rangle$ with $\langle\hat{F}\rangle\langle\hat{G}\rangle$.

First, we do the stability analysis of the fixed points [3] in Eq. (4). The fixed points are the solutions after letting all the first-order derivatives O be zero. Their stability can be judged by the linearized Langevin equations for the quantum fluctuation operators, which can be expressed in the compact matrix form as [8,32]

$$\dot{u}(t) = S(t)u(t) + n(t), \quad (5)$$

where we have defined $u^T(t) = (\delta\hat{X}_1(t),\ \delta\hat{Y}_1(t),\ \delta\hat{X}_2(t),\ \delta\hat{Y}_2(t),\ \delta\hat{q}(t),\ \delta\hat{p}(t))$ and the input noise operators $n^T(t) = (\sqrt{\kappa}\hat{X}_{\mathrm{in},1}(t),\ \sqrt{\kappa}\hat{Y}_{\mathrm{in},1}(t),\ \sqrt{\kappa}\hat{X}_{\mathrm{in},2}(t),\ \sqrt{\kappa}\hat{Y}_{\mathrm{in},2}(t),\ 0,\ \hat{\xi}(t))$, with quadrature operators $\delta\hat{X}_j = \frac{1}{\sqrt{2}}(\delta\hat{c}_j + \delta\hat{c}_j^\dagger)$, $\delta\hat{Y}_j = \frac{1}{\sqrt{2}i}(\delta\hat{c}_j - \delta\hat{c}_j^\dagger)$, and the corresponding Hermitian input noise operators $\hat{X}_{\mathrm{in},j} = \frac{1}{\sqrt{2}}(\hat{c}_{\mathrm{in},j} + \hat{c}_{\mathrm{in},j}^\dagger)$, $\hat{Y}_{\mathrm{in},j} = \frac{1}{\sqrt{2}i}(\hat{c}_{\mathrm{in},j} - \hat{c}_{\mathrm{in},j}^\dagger)$ $(j = 1, 2)$. Furthermore, the coefficient matrix S has the form

$$S(t) = \begin{pmatrix} -\frac{\kappa}{2} & -(\Delta - J) - \frac{g}{2}q & 0 & \frac{g}{2}q & -\frac{g}{2}(y_1 - y_2) & 0 \\ (\Delta - J) + \frac{g}{2}q & -\frac{\kappa}{2} & -\frac{g}{2}q & 0 & \frac{g}{2}(x_1 - x_2) & 0 \\ 0 & \frac{g}{2}q & -\frac{\kappa}{2} & -(\Delta + J) - \frac{g}{2}q & \frac{g}{2}(y_1 - y_2) & 0 \\ -\frac{g}{2}q & 0 & (\Delta + J) + \frac{g}{2}q & -\frac{\kappa}{2} & -\frac{g}{2}(x_1 - x_2) & 0 \\ 0 & 0 & 0 & 0 & 0 & \omega_m \\ g(x_1 - x_2) & g(y_1 - y_2) & -g(x_1 - x_2) & -g(y_1 - y_2) & -\omega_m & -\gamma \end{pmatrix}. \tag{6}$$

Here x_j, y_j are the real part and imaginary part of the complex amplitude c_j $(j = 1, 2)$ respectively. The dynamics of matrix S depends on the time evolution of Eq. (4) under the assumption that the quantum fluctuations always follow the classical orbit, which is guaranteed as long as none of the Lyapunov exponents in the corresponding classical equations is positive [4]. For analysis of the stability, the linearization is performed around the fixed point. The system is stable only if all eigenvalues of matrix S evaluated at the fixed point have negative real parts.

In Fig. 1(a), we choose $2J = \omega_m$ and plot the two-dimensional phase diagram with respect to the driving strength Λ and driving detuning Δ. The system will eventually arrive at the fixed points in region I; by contrast it will settle into the limit cycles in region II. The mechanical freedom in the latter case conducts an approximately sinusoidal oscillation at its unperturbed frequency, i.e., $q(t) = q_0 + A\cos(\omega_m t)$ with shifted equilibrium position q_0 and amplitude A. The threshold value for lasing can be obtained by demanding that the effective mechanical damping rate $\gamma_{\mathrm{eff}} = \gamma_m + \gamma_{\mathrm{opt}} = 0$ [11], where γ_{opt} is the optomechanical damping rate induced by the radiation pressure force. We calculate the mechanical susceptibility [1] and get

$$\gamma_{\mathrm{opt}} = \omega_m|\alpha_2|^2 g^2 \frac{2\kappa\Delta\left[3B^2 - 2B\left(\omega_m^2 + \Delta^2\right) - \left(\omega_m^2 - \Delta^2\right)^2 - B\kappa^2\right]}{[(B - (\omega_m + \Delta)^2]^2 + \kappa^2(\omega_m + \Delta)^2\{[B - (\omega_m - \Delta)^2]^2 + \kappa^2(\omega_m - \Delta)^2\}},$$

with $B = J^2 + \frac{\kappa^2}{4}$, and $\alpha_2 = (c_1 - c_2)/\sqrt{2}$ evaluated at the corresponding fixed point. As shown in Fig. 1(b), γ_{opt} is negative and decreases with driving amplitude. The intersection point of the two lines $\gamma_{\mathrm{opt}}(\Lambda)$ and $-\gamma_m$ indicates the driving threshold Λ_{th}. It becomes larger when the driving detuning goes away from the resonant case $\Delta = J$.

To get more insights into the interplay between nonlinear dynamics and quantum entanglement, we choose three typical paths to cross the boundaries [see Fig. 1(a)]. The long time behavior of the three points marked on path 1 in Fig. 1(a) is explicitly displayed in Fig. 2. All the variables keep constant values at the fixed point (the left point on path 1), while in region II (the middle and right points on path 1) they oscillate with time at the mechanical frequency ω_m. The middle point described in Fig. 2(b) is very close to the boundary, the oscillation for x_1 has only one maximum and one minimum within one cycle. As we move away a little bit from the boundary, the number of oscillation extrema for x_1 doubles [see Fig. 2(c)], developing into the period-2 orbit [33]. In Fig. 3, we plot the mechanical oscillation amplitude A on the three paths. Path 1 in Fig. 3(a) represents the resonant driving of the c_1 mode, with the amplitude starting from $A = 0$, and is an example of a Hopf bifurcation. The amplitude A is proportional to $\sqrt{\Lambda - \Lambda_{th}}$, and the bottom part shows the corresponding new equilibrium position q_0 pushed by the radiation pressure force. The stronger the input driving, the more the mechanical resonator will be shifted. Until, to some extent, it oscillates coherently. Path 2 in Fig. 3(b) goes vertically in the phase diagram, and passes the boundary twice. The amplitude near the boundary has a similar square root relationship as in path 1, i.e., $A \propto \sqrt{|\Delta - \Delta_{th}|}$, where Δ_{th} is the detuning at the boundary. Path 3 in Fig. 3(c) introduces some detuning in the driving of mode c_1. The amplitude A, which is proportional to $\sqrt[4]{\Lambda - \Lambda_{th}}$, increases more rapidly in the vicinity of the threshold than the resonant driving.

IV. QUANTUM ENTANGLEMENT

To check whether there exist quantum signatures of this classical transition, we calculate the degree of quantum entanglement by using the logarithmic negativity [34]. The quantum statistical properties of the system can be investigated through the small fluctuations of the operators around the time-dependent mean values evolving according to Eq. (4). The standard linearization [35] around the classical orbit gives rise to Eq. (5). Since the equations are linear, the fluctuations will remain Gaussian if the input noise is Gaussian. In this case, the properties of quantum fluctuations are fully charac-

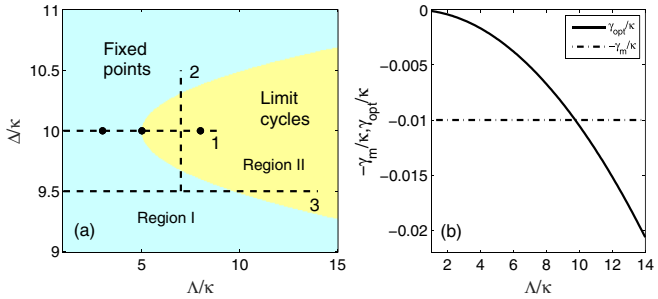

FIG. 1. (a) Phase diagram describing the long-time dynamical behavior of the optomechanical phonon laser with the parameters $J/\kappa = 10$, $\omega_m/\kappa = 20$, $g/\kappa = 0.02$, $\gamma_m/\kappa = 0.01$. The three dashed lines labeled with 1, 2, 3 denote path 1, path 2, and path 3, respectively (path 1: resonant driving of c_1 mode with $\Delta = J$; path 2: going vertically in the diagram with $\Lambda/\kappa = 7$; path 3: driving c_1 mode with detuning $\Delta/\kappa = 9.5$). The time evolution of the three marked points on path 1 from left to right with $\Lambda/\kappa = 3$, 5.01, 8, will be shown below. (b) Calculation of the lasing threshold value (or transition point) for path 3 by finding the intersection point of the two lines $\gamma_{\rm opt}(\Lambda)$ and $-\gamma_m$.

terized by the covariance matrix V, with its elements defined by $V_{ij} = \frac{1}{2}[\langle u_i(t)u_j(t) + u_j(t)u_i(t)\rangle]$. The equation of motion for the covariance matrix is governed by [32]

$$\dot{V}(t) = S(t)V(t) + V(t)S^T(t) + D, \tag{7}$$

where $D = \mathrm{diag}(\frac{\kappa}{2}, \frac{\kappa}{2}, \frac{\kappa}{2}, \frac{\kappa}{2}, 0, \gamma_m(2\bar{n}+1))$ is the diffusion matrix. The optical c_2 mode and the mechanical mode are entangled, and their entanglement is related to the covariance matrix W between these two modes, which is a submatrix of V:

$$W = \begin{pmatrix} V_{33} & V_{34} & V_{35} & V_{36} \\ V_{43} & V_{44} & V_{45} & V_{46} \\ V_{53} & V_{54} & V_{55} & V_{56} \\ V_{63} & V_{64} & V_{65} & V_{66} \end{pmatrix} = \begin{pmatrix} M & C \\ C^T & N \end{pmatrix}, \tag{8}$$

with M, N, C being 2×2 matrices. M and N account for the local properties of the c_2 mode and the mechanical mode, respectively, while C describes intermode correlations. The logarithmic negativity can be obtained with the formula $E_N = \max[0, -\ln 2\eta^-]$, where $\eta^- = 2^{-\frac{1}{2}}\{\sum(W) - [\sum(W)^2 - 4\det W]^{\frac{1}{2}}\}^{\frac{1}{2}}$, and $\sum(W) = \det(M) + \det(N) - 2\det(C)$ [35]. We are interested in the long-time behavior of the entanglement. In our numerical integration of Eqs. (4) and (7), we start with a set of random initial values for V, c_1, c_2, q, p until E_N reaches a steady state. The entanglement in region I will evolve to a constant value, while in the region II it oscillates periodically with the mechanical frequency. Since the quantum fluctuations follow the classical orbit, it is not surprising that the entanglement has similar time dependence as the classical dynamics, either stationary or periodic. The linearization method to calculate the entanglement for limit cycles has been used in several recent works [4,5,7,36]. All of them are discussed in the weak coupling and strong-driving regime. In the opposite case of strong coupling and weak-driving regime, there are works that have shown the phase diffusion phenomenon for limit cycles with a full simulation of the master equations [11,37]. In principle, the random noise will make the steady-state distribution smear out around the circle, in contrast to the point-like picture assumed above. But since in our case the optomechanical coupling is weak and the temperature considered is very low, the influence of noise should be relatively small, leading to much longer transient time before any phase diffusion is significantly likely to happen. In such a case, the point-like picture is still meaningful. The strictest way to check is to do the full simulations of master equations, which is impossible in our parameter regime due to the huge Hilbert space involved. This is an open question and deserves further study.

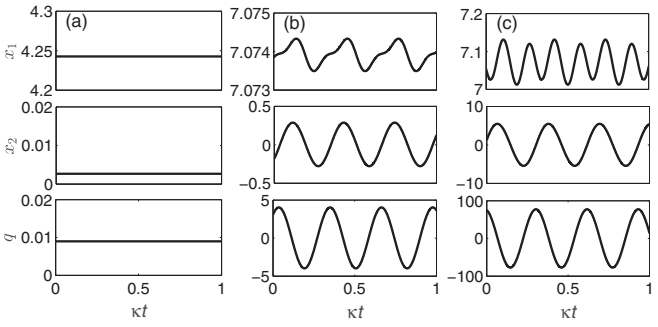

FIG. 2. Long-time dynamical behavior for the three marked points from the left to right in Fig. 1(a) corresponds to panels (a), (b), and (c), respectively, here.

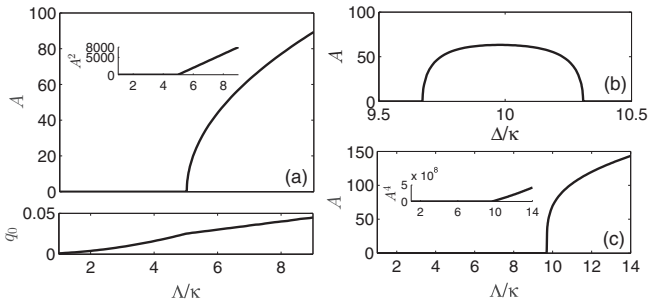

FIG. 3. Mechanical oscillation amplitude A on paths 1, 2, 3 depicted in panels (a), (b), and (c), respectively. The corresponding shifted equilibrium position q_0 on path 1 is also included in panel (a).

In Fig. 4, we plot the steady-state entanglement of the three typical paths at zero temperature. $E_N(t)$ varies over time within a certain range of values, and we denote its maximum and minimum values as $E_{\rm max}$ and $E_{\rm min}$, respectively. The entanglement for path 1 is depicted in Fig. 4(a), where the two lines for $E_{\rm max}$ and $E_{\rm min}$ coincide below the threshold, increase as approaching the transition point, where they start to separate apart more and more with increasing driving amplitude. We give the details of $E_N(t)$ for the three marked points [see Figs. 4(1a), 4(2a), and 4(3a)]. The entanglement for a stable fixed point is a constant and does not change with time. Beyond the threshold, for the point that is close to the boundary, the entanglement $E_N(t)$ oscillates in a symmetric sinusoidal form. As the point moves away from the boundary, $E_N(t)$ gets tilted over time. This is related to the emergence of the period-2 orbit mentioned above. Figure 4(b) shows the

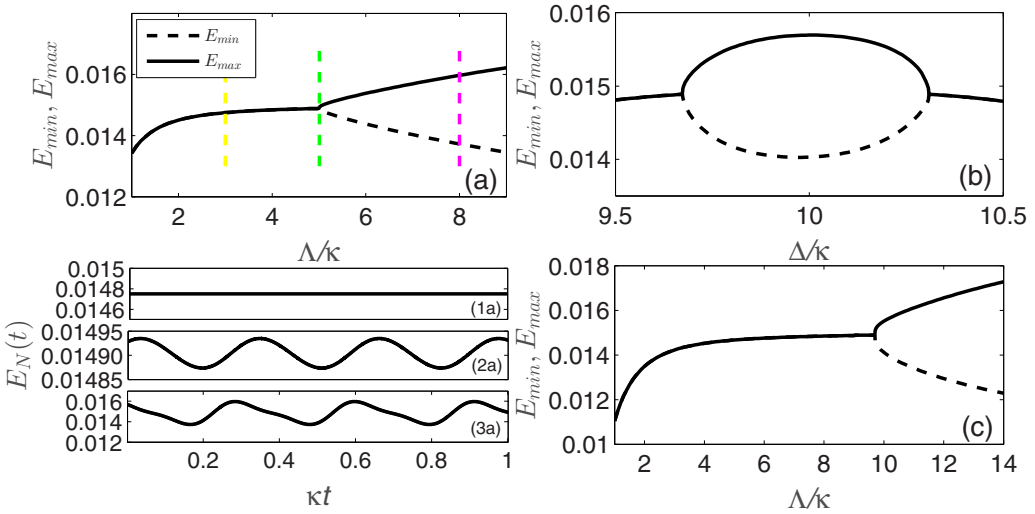

FIG. 4. Steady-state entanglement with $\bar{n} = 0$ for paths 1, 2, 3 plotted in panels (a), (b), and (c), respectively. The details of $E_N(t)$ for the three marked points analyzed above, which also correspond to the three vertical dashed lines in panel (a) from left to right, are shown in panels (1a), (2a), and (3a), respectively.

entanglement for path 2, which has two bifurcations corresponding to passing the boundary twice and also demonstrates the tendency to increase before the bifurcations. The maximum entanglement is achieved at some place in between, where the mechanical oscillation amplitude A is comparatively large. The features for path 3 in Fig. 4(c) are quite similar; however, the change at the bifurcation is much steeper, which is due to the rapid increase of the amplitude A near the threshold.

The most interesting phenomenon is that the entanglement of those points quite close to the boundary line is a constant and is the maximum entanglement for all the stable fixed points, which is a strong quantum fingerprint for the transition from stable fixed points to limit cycles. Here, we emphasize that the points can never be exactly on the boundary due to the numerical discreteness, either on its left side or right side. As shown in Fig. 5, there is a tendency of rapid increase of mechanical fluctuations in a very tiny range approaching the boundary, which makes the linearization methods fail to apply. So we exclude this tiny range in our calculations. However, the nearest points to the boundary (see red stars in Fig. 5) we have chosen are good enough to indicate the transition position. Note that, although the parameter values in region I of Fig. 1(a) are all for stable fixed points, the positions of the fixed points in the parameter space are generally different. In particular, the four points closest to the boundary that the three paths in Fig. 1(a) encounter have different positions, but they have the same entanglement. We have also checked randomly many other points quite close to the boundary: the entanglement remains the same. For the parameters chosen in Fig. 4, the constant is about 0.014 88. We guess this should be related to the function of the boundary line, which is contained in the expression of the entanglement and leads to a constant value just quite near the boundary. But the analytical calculation of this entanglement is too complicated for our model.

We now consider the influence from the temperature. The entanglement of path 1 and path 2 with different mean thermal phonon numbers is given by Fig. 6. The entanglement on both sides of the transition point falls down obviously with the increase of temperature, while the entanglement quite near the boundary is very robust against the presence of thermal mechanical noise. It decreases relatively slower with rising temperature, but keeps constant along the boundary line. In

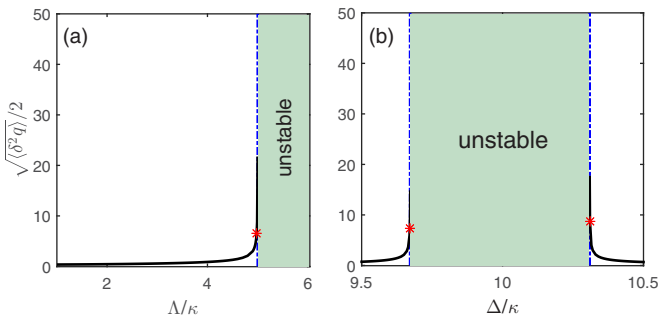

FIG. 5. Mechanical fluctuation radius $\frac{1}{2}(\langle\delta^2\hat{q}\rangle)^{1/2}$ $[\simeq\frac{1}{2}(\langle\delta^2\hat{p}\rangle)^{1/2}]$ for stable fixed points of path 1 and path 2 shown in panels (a) and (b), respectively. Dashed lines are the boundary lines and red stars are the nearest points to the boundary chosen in our numerical calculations.

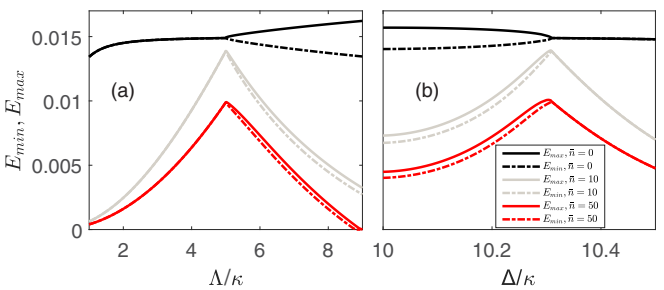

FIG. 6. Temperature influence of the steady-state entanglement for path 1 in panel (a) and path 2 in panel (b).

the limit cycle region, the difference between the maximum and minimum of entanglement, i.e., $E_{\max} - E_{\min}$, also decreases with higher temperature. $E_{\min}$ touches zero first, and then $E_{\max}$ follows, which means that there is no entanglement any more; for example, the situation in Fig. 6(a) with $\Lambda/\kappa = 9$ and $\bar{n} = 50$.

V. CONCLUSION

To summarize, we have studied how the quantum entanglement changes from stable fixed points to limit cycles in an optomechanical phonon laser system, with the aim of finding the quantum signatures of these particular nonlinear dynamical transitions. We pick out three different paths to cross the boundary and analyze their nonlinear dynamics and quantum entanglement properties. Our calculations show that, indeed, there are some quantum features in common to indicate this classical transition: (1) The quantum entanglement for the stable fixed points is a constant number, whereas it oscillates in time at the mechanical frequency for the limit cycles. The transition point is where this oscillation starts to happen. (2) The entanglement of the stable fixed points increases upon approaching the transition boundary and reaches the maximum value quite close to the boundary. Most strikingly, the entanglement of those points quite close to the boundary line is a constant, which is a strong signal for the indication of the transition border line. (3) The entanglement around the boundary line is very robust against the influence of thermal noise, so that it decreases relatively slower with increasing temperature. Furthermore, even at finite temperature, although the entanglement decreases, it has the same value along the boundary line. Thus we can still easily find out the transition boundary by the amount of quantum entanglement. In a word, we have investigated the fundamental problem of quantum manifestations of transition between different types of motions in nonlinear dynamical systems, which deserves much more effort in the future for transitions between other more complex dynamical behavior.

ACKNOWLEDGMENTS

Z.J.D. is grateful to Florian Marquardt, Ying-Cheng Lai, Talitha Weiss, and Jie-Qiao Liao for useful discussions. This work was supported by the National Natural Science Foundation of China under Grants No. 11574398, No. 11775101, and No. 61632021, the National Basic Research Program of China under Grant No. 2016YFA0301903, and by the Natural Science Foundation of Hunan Province of China under Grant No. 2018JJ2467.

[1] M. Aspelmeyer, T. J. Kippenberg, and F. Marquardt, Rev. Mod. Phys. **86**, 1391 (2014).
[2] M. Aspelmeyer, P. Meystre, and Keith Schwab, Phys. Today **65**(7), 29 (2012).
[3] S. H. Strogatz, *Nonlinear Dynamics and Chaos* (Perseus Publishing, Cambridge, 1994).
[4] G. Wang, L. Huang, Y.-C. Lai, and C. Grebogi, Phys. Rev. Lett. **112**, 110406 (2014).
[5] L. Ying, Y.-C. Lai, and C. Grebogi, Phys. Rev. A **90**, 053810 (2014).
[6] A. Mari, A. Farace, N. Didier, V. Giovannetti, and R. Fazio, Phys. Rev. Lett. **111**, 103605 (2013).
[7] F. Bemani, A. Motazedifard, R. Roknizadeh, M. H. Naderi, and D. Vitali, Phys. Rev. A **96**, 023805 (2017).
[8] R. Ghobadi, A. R. Bahrampour, and C. Simon, Phys. Rev. A **84**, 033846 (2011).
[9] I. S. Grudinin, H. Lee, O. Painter, and Kerry J. Vahala, Phys. Rev. Lett. **104**, 083901 (2010).
[10] F. Marquardt, J. G. E. Harris, and S. M. Girvin, Phys. Rev. Lett. **96**, 103901 (2006).
[11] M. Ludwig, B. Kubala, and F. Marquardt, New J. Phys. **10**, 095013 (2008).
[12] H. Wu, G. Heinrich, and F. Marquardt, New J. Phys. **15**, 123022 (2013).
[13] R. Lauter, C. Brendel, S. J. M. Habraken, and F. Marquardt, Phys. Rev. E **92**, 012902 (2015).
[14] T. Weiss, A. Kronwald, and F. Marquardt, New J. Phys. **18**, 013043 (2016).
[15] N. Lörch and K. Hammerer, Phys. Rev. A **91**, 061803(R) (2015).
[16] L. Bakemeier, A. Alvermann, and H. Fehske, Phys. Rev. Lett. **114**, 013601 (2015).
[17] C. Wurl, A. Alvermann, and H. Fehske, Phys. Rev. A **94**, 063860 (2016).
[18] R. Huang and H. Jing, Nat. Photonics **13**, 372 (2019).
[19] S. Zaitsev, A. K. Pandey, O. Shtempluck, and E. Buks, Phys. Rev. E **84**, 046605 (2011).
[20] R. M. Pettit, W. Ge, P. Kumar, D. R. Luntz-Martin, J. T. Schultz, L. P. Neukirch, M. Bhattacharya, and A. N. Vamivakas, Nat. Photonics **13**, 402 (2019).
[21] D. F. Walls and G. J. Milburn, *Quantum Optics*, 2nd ed. (Springer-Verlag, Berlin-Heidelberg, 2008).
[22] C. W. Gardiner and M. J. Collett, Phys. Rev. A **31**, 3761 (1985).
[23] V. Giovannetti and D. Vitali, Phys. Rev. A **63**, 023812 (2001).
[24] M. Schmidt, M. Ludwig, and F. Marquardt, New J. Phys. **14**, 125005 (2012).
[25] Y.-D. Wang and A. A. Clerk, Phys. Rev. Lett. **110**, 253601 (2013).
[26] L. Tian, Phys. Rev. Lett. **110**, 233602 (2013).
[27] Y.-D. Wang, S. Chesi, and A. A. Clerk, Phys. Rev. A **91**, 013807 (2015).
[28] Z. J. Deng, S. J. M. Habraken, and F. Marquardt, New J. Phys. **18**, 063022 (2016).
[29] Z. J. Deng, X.-B. Yan, Y.-D. Wang, and C.-W. Wu, Phys. Rev. A **93**, 033842 (2016).
[30] X.-B. Yan, Z. J. Deng, X.-D. Tian, and J.-H. Wu, Opt. Express **27**, 24393 (2019).
[31] R. Zhang, Y. Fang, Y.-Y. Wang, S. Chesi, and Y.-D. Wang, Phys. Rev. A **99**, 043805 (2019).
[32] A. Mari and J. Eisert, Phys. Rev. Lett. **103**, 213603 (2009).
[33] E. Ott, *Chaos in Nonlinear Dynamics* (Cambridge University Press, Cambridge, 1993).

[34] G. Vidal and R. F. Werner, Phys. Rev. A **65**, 032314 (2002).

[35] D. Vitali, S. Gigan, A. Ferreira, H. R. Böhm, P. Tombesi, A. Guerreiro, V. Vedral, A. Zeilinger, and M. Aspelmeyer, Phys. Rev. Lett. **98**, 030405 (2007).

[36] C.-S. Hu, L.-T. Shen, Z.-B. Yang, H. Wu, Y. Li, and S.-B. Zheng, Phys. Rev. A **100**, 043824 (2019).

[37] J. Qian, A. A. Clerk, K. Hammerer, and F. Marquardt, Phys. Rev. Lett. **109**, 253601 (2012).